*International Journal of Innovative Computing, Information and Control*
Volume **22**, Number **3**, June **2026**

ICIC International ©2026 ISSN 1349-4198
pp. **579–597**

# A VALIDATED 8-DOF BIOMECHANICAL MODEL FOR VIBRATION ANALYSIS IN OCCUPANT-WHEELCHAIR SYSTEMS WITH COMMERCIAL CUSHION INTEGRATION

Mitsuki Katahira[1], Pongtep Weerapong[2,*], Md Abdus Samad Kamal[3]
Iwanori Murakami[3] and Kou Yamada[3]

[1]Graduate School of Science and Technology
[3]Division of Mechanical Science and Technology
Gunma University
1-5-1 Tenjincho, Kiryu 376-8515, Japan
{ t221b020; maskamal; murakami; yamada }@gunma-u.ac.jp

[2]Department of Production Technology
Faculty of Industrial Technology
Nakhon Si Thammarat Rajabhat University
1 M.4, Tha Ngio, Mueang Nakhon Si Thammarat, Nakhon Si Thammarat 80280, Thailand
[*]Corresponding author: pongtap_wee@nstru.ac.th

Received August 2025; revised November 2025

Abstract. *This paper presents an advanced biomechanical model with eight degrees of freedom (8-DOF) to rigorously characterize the dynamic interactions between wheelchair occupants and seating systems. In contrast to traditional single- or two degree of freedom (SDOF/TDOF) approaches that oversimplify occupant-seat coupling, the proposed 8-DOF framework explicitly resolves the complex mechanical pathways governing vibration transmission through anatomical and structural subsystems. By incorporating precisely calibrated stiffness and damping parameters derived from seven commercial wheelchair cushions, the model achieves high fidelity in predicting seat-to-occupant transmissibility across the critical 0-20 [Hz] frequency range. Experimental validation using real-world Wheelchair Road Course (WRC) data confirms that the model reliably reproduces biomechanical responses under realistic excitation. Notably, cushions with low stiffness and low damping produced amplified transmissibility peaks near 3-4 [Hz] – a range corresponding to human vertical resonance – while designs with optimized damping-stiffness combinations effectively mitigated these vibrations. These findings emphasize the pivotal role of energy dissipation in preventing resonance amplification and promoting long-term user comfort. The validated 8-DOF framework thus offers mechanical, computational, and translational advantages, serving as a robust tool for designing next-generation seating systems that balance biomechanical protection with engineering performance.*
**Keywords:** Occupant-wheelchair dynamics, Vibration transmissibility, Dynamic stiffness and damping, Cushion evaluation, Multibody biomechanical modeling

1. **Introduction.** The dynamic interaction between wheelchair users and ground-induced vibrations remains a critical concern in biomechanical engineering [1, 2], particularly for individuals with limited postural control or those exposed to long durations of seated mobility. Unlike vehicular suspension systems, manual wheelchairs rely primarily on passive components – namely, the mechanical characteristics of seat cushions and frames – to attenuate terrain-induced vibration [3, 4]. Vibrations within the low-frequency range of 2-6 [Hz], which coincide with the natural resonance frequencies of the human torso

DOI: 10.24507/ijicic.22.03.579

and internal organs, are known to cause discomfort, postural instability, and long-term musculoskeletal degeneration [5, 6].

In recent years, wheelchair seat cushions have undergone continuous material and structural innovations; however, a system-level understanding of how their dynamic properties, particularly stiffness and damping, govern vibration transmissibility across the full frequency spectrum remains limited [7, 8, 9, 10]. Many earlier investigations relied on highly simplified modeling frameworks or laboratory-based test setups. In particular, simplified SDOF or TDOF models, together with bench-top experiments using systems such as the material testing system (MTS), were widely employed to characterize cushion response [11, 12, 13]. Although these approaches provided useful preliminary insights, they were inherently based on coarse biomechanical assumptions and frequently failed to reproduce the real-world driving dynamics experienced by wheelchair users [14, 15]. Moreover, the frequent use of nondisabled subjects and idealized excitation inputs further limited the external validity and applicability of these models [16].

Within this context, early SDOF and TDOF formulations typically represented the occupant-seat system as a single lumped mass-spring-damper structure, effectively capturing only a seat-dominated response while implicitly assuming rigid-body behavior of the seated human [11, 12]. To improve realism, subsequent developments introduced biomechanical models with four to six degrees of freedom, in which partial segmentation of the seated human body was incorporated. In these intermediate formulations, components such as the pelvis, trunk, and seat were treated as distinct subsystems in order to capture additional motion modes and improve the description of vibration transmission pathways. As a result, 4-6 DOF models enabled a more explicit representation of seat-pelvis and pelvis-torso interactions and provided improved estimates of low-frequency vibration responses compared with purely lumped representations [17].

Despite these advances, four- to six-degree-of-freedom models remain inherently limited when applied to authentic operating conditions. Experimental and field-based investigations have shown that vibration transmission in wheelchair users is strongly influenced by coupled biomechanical interactions that are not explicitly resolved in such reduced-order models. In particular, the dynamic coupling between the pelvis and the compliant seat cushion, the interaction between cushion deformation and wheelchair frame flexibility, and the resonance behavior of the upper torso and head-neck system play a dominant role during real-world propulsion and terrain-induced excitation [14, 15, 16]. Because these interactions are only partially represented in intermediate-complexity models, vibration amplification phenomena observed in practice, especially within low-frequency ranges associated with heightened biodynamic sensitivity, are often underestimated or smeared.

These unresolved limitations collectively motivate the need for a higher-resolution biomechanical representation that remains physically interpretable while avoiding unnecessary complexity. Accordingly, the present study adopts an 8-DOF biomechanical model as a minimal-complete description of the occupant-wheelchair system. The proposed 8-DOF formulation is not intended to be overcomplicated; rather, it is deliberately selected to be minimal yet sufficient to capture the essential biomechanical couplings among the seat cushion, wheelchair structure, and anatomically segmented human body components. By explicitly resolving pelvis-seat interaction, cushion-frame compliance, and upper-body resonance within a unified framework, the model extends beyond lumped and partially segmented representations while remaining the simplest configuration capable of representing seat-pelvis-trunk-head dynamics in a physically consistent manner.

Nevertheless, whether based on simplified DOF representations or idealized experimental configurations, many existing approaches continue to fall short in replicating authentic real-world driving conditions. Such models frequently introduce systematic inaccuracies

due to oversimplified biomechanical assumptions [14, 15], while the reliance on nondisabled subjects and artificially controlled excitation signals further constrains their relevance to actual wheelchair users [16].

Recent paper highlights the critical importance of advanced biomechanical modeling in accurately representing wheelchair vibration dynamics. Luo et al. [18] conducted extensive simulations and experimental analyses examining occupant stability and comfort over irregular surfaces, emphasizing the influential role of cushion characteristics. Chadefaux et al. [19] identified persistent limitations of conventional modeling approaches, revealing notable discrepancies compared to vibration exposures experienced by wheelchair users under realistic conditions. Additionally, Cui et al. [20] highlighted increasing complexities in human-seat interactions through advanced multimodal human-computer interface technologies. Despite these valuable insights, current biomechanical frameworks still lack comprehensive integration of experimental transmissibility data with detailed multibody dynamic analyses across various cushion types.

More recently, Larivière et al. [21] confirmed that ground surface types, propulsion techniques, and driving speed significantly influence vibration levels, underscoring the need for in-situ evaluations rather than laboratory simplifications. Neti et al. [22] demonstrated that even advanced mechanical suspension systems implemented at the wheel level do not fully mitigate vibrations without corresponding optimization of the cushion-body interface. Moreover, Zhang et al. [23] used a hybrid artificial neural network-genetic algorithm framework to predict transmissibility characteristics, though their method still lacked validation against dynamic real-world inputs.

Taken collectively, these findings reveal three persistent and intertwined research gaps: 1) the absence of a validated vibration model that integrates cushion-specific stiffness and damping parameters representative of commercial products; 2) the inadequate biomechanical segmentation of the seated human body in existing models, which obscures resonance behavior within the 3-4 [Hz] zone of high biodynamic sensitivity; and 3) a lack of reliable experimental validation under authentic driving conditions such as those simulated by WRC, which provides in-situ transmissibility profiles across heterogeneous terrains.

To address these challenges, the present study proposes a high-resolution 8-DOF linear biomechanical vibration model of the occupant-wheelchair system. This model features anatomically segmented occupant components (lower torso, viscera, upper torso, and head-neck) and mechanical representations of the wheelchair (wheel assemblies, frame, and cushion). Seven commercial seat cushions are each characterized by uniquely calibrated stiffness and damping parameters derived from field-based WRC transmissibility measurements. This enables the model to simulate vibration transmission under realistic base excitations and anatomical coupling.

Unlike prior SDOF/TDOF frameworks, the proposed 8-DOF system captures the propagation of vibrational energy across multiple structural and anatomical layers and resolves transmissibility behavior over the entire 0-20 [Hz] operational frequency range. Experimental comparisons demonstrate that the model reproduces the overall frequency-dependent transmissibility characteristics across 0-20 [Hz]. The weighted root-mean-square (RMS) error, expressed as Deviation [%], is evaluated over the full frequency band and ranges from 8.34-52.70 [%] depending on the cushion configuration. The larger deviations occur primarily in resonance-sensitive cases within the 3-4 [Hz] biodynamic region, where small shifts in peak frequency or amplitude significantly influence percentage-based error metrics. Despite these localized discrepancies, the model consistently preserves the dominant transmissibility trends, relative peak ordering, and frequency-dependent dynamic behavior across all cushion configurations.

Such detailed modeling frameworks, exemplified by the 8-DOF approach proposed herein, allow engineers to understand and accurately predict how vibrations propagate through each occupant body segment, cushion, and wheelchair component under realistic operating conditions [1, 24]. In practice, the model supports comparative performance classification of cushions, evidence-based design optimization, and clinical decision-making for minimizing exposure to harmful vibration ranges.

This paper is organized as follows. Section 2 outlines the mechanical segmentation of the system and the spring-damper formulations. Section 3 presents the equations of motion and frequency-domain transformations. Section 4 provides detailed simulation-experiment comparisons across seven cushion types. Finally, Section 5 concludes the findings and proposes future directions in adaptive cushion design and biomechanical modeling.

## 2. Dynamic Formulation and Model Development of the 8-DOF Occupant-Wheelchair System.

2.1. **Lumped-parameter architecture for vibration transmission analysis.** To accurately characterize vibration transmission between wheelchair structural components and human body segments during seated exposure, an eight-degree-of-freedom lumped-parameter biomechanical model is established. This framework integrates the primary mechanical and anatomical subsystems involved in vertical vibration propagation, while preserving the essential dynamic coupling pathways required for transmissibility evaluation under realistic operating conditions.

The system response is described in terms of the vertical displacement coordinates $z_1$ through $z_8$, each corresponding to a physically distinct subsystem illustrated in Figure 1. Specifically, $z_1$ and $z_2$ denote the vertical displacements of the front and rear tire assemblies, respectively, which represent the primary interfaces between the wheelchair and the ground. The coordinate $z_3$ corresponds to the vertical motion of the wheelchair suspension and frame assembly, capturing structural compliance between the wheels and the seating system. The displacement $z_4$ represents the vertical response of the seat and cushion subsystem, which governs the mechanical interaction between the wheelchair structure and the seated occupant.

The remaining displacement coordinates describe the biomechanical response of the occupant. The variable $z_5$ denotes the vertical motion of the lower torso (pelvic region), which is directly coupled to the seat cushion. The coordinate $z_6$ represents the viscera, accounting for internal mass motion within the abdomen. The variable $z_7$ corresponds to the upper torso, while $z_8$ denotes the vertical displacement of the head-neck system, which is critical for evaluating upper-body resonance and vibration amplification.

Accordingly, the model partitions the overall system into two main groups of subsystems: wheelchair mechanical components, comprising the front tires ($m_1$), rear tires ($m_2$), suspension and frame ($m_3$), and seat cushion ($m_4$); and occupant biomechanical components, comprising the lower torso ($m_5$), viscera ($m_6$), upper torso ($m_7$), and head-neck ($m_8$). Adjacent subsystems are interconnected by linear springs and dampers, representing elastic restoring forces and energy dissipation, respectively. The complete coupling structure along the vertical vibration transmission path is illustrated schematically in Figure 1.

2.2. **Vertical base excitation modeling.** The system is subjected to harmonic road-induced excitation, which is modeled as a sinusoidal vertical base displacement applied at the tire-ground contact points:

$$z_0(t) = A\sin(\omega t), \tag{1}$$

where $A$ denotes the excitation amplitude and $\omega$ represents the angular frequency in rad/s.

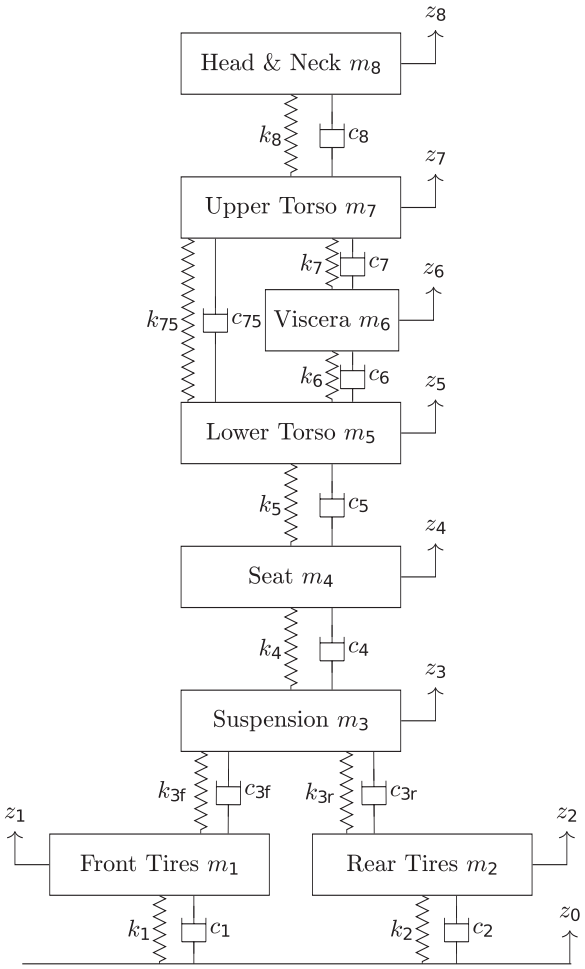


FIGURE 1. The lumped-parameter 8-DOF occupant-wheelchair vibration model subjected to vertical base excitation, showing the associated displacement coordinates $z_1$-$z_8$ for each mechanical and biomechanical subsystem

This excitation model reflects typical vibrational conditions encountered during real-world wheelchair operation over uneven surfaces. In accordance with prior experimental and numerical investigations, vibration transmission through the footrests is neglected due to its negligible contribution to the overall vertical dynamic response [15, 16].

2.3. **Mechanical property identification.** The lumped mass, stiffness, and damping parameters are extracted from validated experimental, anatomical, and biomechanical literature sources [1, 10, 14]. The identified parameters for both the mechanical wheelchair structure and the occupant's anatomical segments are summarized in Tables 1 and 2.

The mechanical properties of human tissues used in this paper are adapted from validated anatomical and biomechanical sources such as [1, 10, 14] and summarized in Table 1. The wheelchair is modeled as a standard manual type commonly used in urban settings.

The occupant is assumed to sit without upper body restraint, supported only by the cushion system. Vibratory inputs are modeled as sinusoidal base excitations transmitted from road surface irregularities through the tire-frame-seat structure. These vibrations primarily travel through the seat cushion, whose mechanical configuration significantly affects how energy is transmitted to the occupant's body [2, 7, 9].

TABLE 1. Dynamic properties of the primary 8-DOF occupant-wheelchair model components

| Component | Mass [kg] | Damping constant [N·s/m] | Stiffness constant [N/m] |
|---|---|---|---|
| Front tire | $m_1 = 1.00$ | $c_1 = 500$ | $k_1 = 60{,}000$ |
| Rear tire | $m_2 = 1.60$ | $c_2 = 500$ | $k_2 = 6{,}000$ |
| Suspension | $m_3 = 15.00$ | $c_{3f} = 700$<br>$c_{3r} = 700$ | $k_{3f} = 13{,}400$<br>$k_{3r} = 74{,}600$ |
| Seat cushion | $m_4 = 1.50$ | Defined per model variant (see Table 2) | |
| Lower torso | $m_5 = 36.00$ | $c_5 = 2{,}475$ | $k_5 = 49{,}340$ |
| Viscera | $m_6 = 5.50$ | $c_6 = 330$ | $k_6 = 20{,}000$ |
| Upper torso | $m_7 = 15.00$ | $c_7 = 200$ | $k_7 = 10{,}000$ |
| Head & neck | $m_8 = 4.17$ | $c_8 = 250$ | $k_8 = 134{,}400$ |
| Upper-lower torso joint | – | $c_{75} = 909.1$ | $k_{75} = 192{,}000$ |

**Denotations:** $m_i$ denotes the lumped mass of the $i$-th segment; $c_i$ and $k_i$ represent the damping and stiffness coefficients, respectively. Subscripts $f$ and $r$ denote front and rear components. The base excitation amplitude is set to $A = 0.005$ [m], following ISO 2631-1:1997 [25].

TABLE 2. Calibrated dynamic properties of commercial seat cushion variants (all cushions assumed to have a mass ($m_4$) of 1.50 [kg])

| Seat cushion | Damping constant [N·s/m] | Stiffness constant [N/m] |
|---|---|---|
| Jay J2 Deep Contour | $c_4 = 571$ | $k_4 = 39{,}970$ |
| Meridian Wave | $c_4 = 397$ | $k_4 = 76{,}010$ |
| ROHO High Profile | $c_4 = 834$ | $k_4 = 94{,}220$ |
| Vector with Vicair | $c_4 = 840$ | $k_4 = 95{,}040$ |
| ROHO Low Profile | $c_4 = 1{,}015$ | $k_4 = 68{,}600$ |
| Zoombang Protective Gear with Foam | $c_4 = 1{,}507$ | $k_4 = 174{,}900$ |
| Comfort Mate Foam | $c_4 = 1{,}689$ | $k_4 = 183{,}200$ |

Figure 1 depicts the complete lumped-parameter system, consisting of eight interconnected masses, springs, and dampers. Each segment is defined by its mechanical impedance properties, with interaction between seat and human tissues carefully modeled to reflect real-world response characteristics. The influence of footrests is neglected due to their minimal contribution to vertical vibration transmission [15, 16].

This mathematical framework enables direct analysis of transmissibility behavior across frequency bands relevant to human body resonance (2-6 [Hz]) [5, 6], and is further calibrated using WRC experimental data [2].

3. **Comprehensive Dynamic Modeling and Analytical Formulation of the 8-DOF Occupant-Wheelchair Vibration System.** This section establishes a comprehensive mathematical framework for modeling vibration transmissibility in a seated occupant-wheelchair system, incorporating 8-DOF. The formulation extends prior biomechanical and whole-body vibration (WBV) models [1, 2, 11, 14, 15], providing a higher-fidelity representation by integrating both mechanical structure and human anatomical segments through Newtonian mechanics and Laplace-domain analysis [3, 7].

3.1. **System configuration and model description.** The overall configuration of the wheelchair-occupant vibration system follows the lumped-parameter architecture established in Section 2.1. In particular, the eight-degree-of-freedom model consists of eight physically distinct subsystems, whose mass definitions are adopted directly from the model formulation described previously.

Specifically, the wheelchair mechanical subsystems comprise the front tire assembly ($m_1$), rear tire assembly ($m_2$), suspension and frame assembly ($m_3$), and seat cushion subsystem ($m_4$), as defined in Section 2.1. The occupant biomechanical subsystems consist of the lower torso ($m_5$), viscera ($m_6$), upper torso ($m_7$), and head-neck system ($m_8$), following the same definitions introduced in the lumped-parameter architecture.

Each lumped mass is interconnected with its adjacent subsystems through linear springs and viscous dampers, which represent elastic restoring forces and energy dissipation associated with tissue deformation, seat compliance, and structural interfaces. This unified configuration ensures consistency between the model formulation and the parameter identification procedures, thereby preserving the physical interpretation of all system components throughout the manuscript.

3.2. **Parameter definition and coupling topology.** All mass parameters ($m_1$-$m_8$) and displacement coordinates ($z_1$-$z_8$) are defined in Section 2.1 and are not redefined in this subsection. Instead, the present section focuses exclusively on specifying the coupling topology of the system and clarifying the functional roles of the associated stiffness and damping parameters within the established eight-degree-of-freedom (8-DOF) framework. Based on the system configuration described in Section 3.1, adjacent subsystems are interconnected through linear spring-damper elements that govern vertical vibration transmission along the ground-wheel-frame-cushion-occupant pathway. Each spring element represents an elastic load-transfer mechanism, while each damper characterizes energy dissipation arising from material hysteresis, interfacial friction, and viscoelastic behavior of soft biological tissues.

The stiffness and damping parameters are grouped according to their corresponding physical interfaces to preserve clear biomechanical and mechanical interpretations. In particular, the tire-ground and wheel-suspension interfaces define the initial vibration input pathway; the suspension-seat and seat-pelvis interfaces regulate vibration transmission into the occupant; and the inter-segment couplings within the human body (pelvis, viscera, upper torso, and head-neck) capture internal biodynamic interactions. This hierarchical coupling structure reflects the dominant vibration propagation mechanisms observed under realistic wheelchair operating conditions.

To ensure numerical robustness and physical plausibility during subsequent parameter identification, all stiffness and damping coefficients are constrained to remain positive and are treated as frequency-independent linear parameters. Such a formulation enables systematic calibration of the model while maintaining a direct correspondence between optimized parameters and physically meaningful properties of the wheelchair components and human body segments. This parameter definition and coupling topology provide a consistent foundation for the derivation of the equations of motion and for the optimization-based parameter identification procedure presented in the following subsections.

3.3. **Time-domain governing equations of motion.** The complete system dynamics are governed by the second-order matrix differential equation:

$$[M]\ddot{z}(t) + [C]\dot{z}(t) + [K]z(t) = f(t), \tag{2}$$

where $[M] \in \mathbb{R}^{8\times8}$ is the lumped mass matrix, reflecting both occupant segmental masses and wheelchair structural components; $[C] \in \mathbb{R}^{8\times8}$ is the damping matrix incorporating viscoelastic properties of soft tissues, cushion materials, and structural interfaces; $[K] \in \mathbb{R}^{8\times8}$ is the stiffness matrix describing elastic restoring forces throughout the coupled system; $z(t)$ represents the displacement vector across the eight DOFs, and $f(t)$ contains externally applied excitations derived from road-induced disturbances.

The system response is evaluated under the harmonic road-induced base excitation defined in Equation (1). The corresponding input force vector becomes

$$f(t) = \begin{bmatrix} c_1\dot{z}_0(t) + k_1 z_0(t) \\ c_2\dot{z}_0(t) + k_2 z_0(t) \\ 0 \\ 0 \\ 0 \\ 0 \\ 0 \\ 0 \end{bmatrix}. \tag{3}$$

3.4. **Frequency-domain formulation via Laplace transform.** Applying Laplace transform under zero initial conditions converts Equation (2) into

$$\left[s^2M + sC + K\right] Z(s) = F(s), \tag{4}$$

where $Z(s)$ and $F(s)$ are Laplace transforms of $z(t)$ and $f(t)$, respectively.

Defining the impedance matrix

$$[Z_{\text{imp}}(s)] = s^2M + sC + K \tag{5}$$

yields the general frequency-domain solution

$$Z(s) = [Z_{\text{imp}}(s)]^{-1}F(s). \tag{6}$$

3.5. **Steady-state harmonic response.** For harmonic steady-state input, substitution $s = j\omega$ gives

$$Z(j\omega) = \left[-\omega^2M + j\omega C + K\right]^{-1} F(j\omega). \tag{7}$$

This equation enables direct frequency-response computations over the excitation spectrum.

3.6. **Explicit expanded formulation.** The system can be further represented in expanded block form:

$$\mathbf{A}(s) \cdot \mathbf{Z}(s) = \mathbf{K}_{\text{input}} Z_0(s), \tag{8}$$

where $\mathbf{A}(s)$ is the full $8 \times 8$ coefficient matrix whose elements combine $m_i$, $c_i$, $k_i$, and coupling terms for each interconnected DOF.

$$\begin{bmatrix} A_1 & 0 & A_2 & 0 & 0 & 0 & 0 & 0 \\ 0 & B_1 & B_2 & 0 & 0 & 0 & 0 & 0 \\ C_1 & C_2 & C_3 & C_4 & 0 & 0 & 0 & 0 \\ 0 & 0 & D_1 & D_2 & D_3 & 0 & 0 & 0 \\ 0 & 0 & 0 & E_1 & E_2 & E_3 & 0 & 0 \\ 0 & 0 & 0 & 0 & F_1 & F_2 & F_3 & 0 \\ 0 & 0 & 0 & 0 & 0 & G_1 & G_2 & G_3 \\ 0 & 0 & 0 & 0 & 0 & 0 & H_1 & H_2 \end{bmatrix} \begin{bmatrix} Z_1(s) \\ Z_2(s) \\ Z_3(s) \\ Z_4(s) \\ Z_5(s) \\ Z_6(s) \\ Z_7(s) \\ Z_8(s) \end{bmatrix} = \begin{bmatrix} K_1 \\ K_2 \\ 0 \\ 0 \\ 0 \\ 0 \\ 0 \\ 0 \end{bmatrix} Z_0(s). \tag{9}$$

Here,

$$
\begin{aligned}
&A_1 = m_1 s^2 + (c_1 + c_{3f})s + (k_1 + k_{3f}), && A_2 = -c_{3f}s - k_{3f},\\
&B_1 = m_2 s^2 + (c_2 + c_{3r})s + (k_2 + k_{3r}), && B_2 = -c_{3r}s - k_{3r},\\
&C_1 = -c_{3f}s - k_{3f}, && C_2 = -c_{3r}s - k_{3r},\\
&C_3 = m_3 s^2 + (c_{3f} + c_{3r} + c_4)s + (k_{3f} + k_{3r} + k_4), && C_4 = -c_4 s - k_4,\\
&D_1 = -c_4 s - k_4, && D_2 = m_4 s^2 + (c_4 + c_5)s + (k_4 + k_5),\\
&D_3 = -c_5 s - k_5, && E_1 = -c_5 s - k_5,\\
&E_2 = m_5 s^2 + (c_5 + c_6 + c_{75})s + (k_5 + k_6 + k_{75}), && E_3 = -c_6 s - k_6,\\
&F_1 = -c_6 s - k_6, && F_2 = m_6 s^2 + (c_6 + c_7)s + (k_6 + k_7),\\
&F_3 = -c_7 s - k_7, &&\\
&G_1 = -c_{75} s - k_{75}, && G_2 = -c_7 s - k_7,\\
&G_3 = m_7 s^2 + (c_7 + c_8 + c_{75})s + (k_7 + k_8 + k_{75}), &&\\
&H_1 = -c_8 s - k_8, && H_2 = m_8 s^2 + c_8 s + k_8,\\
&K_1 = c_1 s + k_1, && K_2 = c_2 s + k_2.
\end{aligned}
$$

3.7. **General transfer function derivation.** The transfer function for the $k$-th output response to the $l$-th input excitation is defined as

$$H_{kl}(j\omega) = \frac{Z_k(j\omega)}{F_l(j\omega)} = \frac{1}{-\omega^2 m_{kl} + j\omega c_{kl} + k_{kl}}, \tag{10}$$

where $m_{kl}$, $c_{kl}$, and $k_{kl}$ denote the equivalent effective parameters governing dynamic coupling between corresponding DOFs.

Assembling the set of all such frequency-domain transfer functions yields the complete $8 \times 8$ transfer function matrix

$$\mathbf{H}(j\omega) = \begin{bmatrix} H_{11}(j\omega) & \cdots & H_{18}(j\omega) \\ \vdots & \ddots & \vdots \\ H_{81}(j\omega) & \cdots & H_{88}(j\omega) \end{bmatrix} = \mathbf{Z}(j\omega)\mathbf{F}(j\omega)^{-1}, \tag{11}$$

where $\mathbf{Z}(j\omega)$ is the vector of frequency-domain displacements and $\mathbf{F}(j\omega)$ is the corresponding excitation vector. This formulation enables the prediction of system response at all DOFs due to arbitrary input excitations, providing a complete characterization of the system's vibration transmission behavior.

3.8. **Physical interpretation and practical insights.** The impedance-based modeling approach described herein offers a robust analytical framework for understanding vibration propagation through the occupant-wheelchair interface. Each transfer function element $H_{kl}(j\omega)$ quantifies how the vibrational energy originating at a specific subsystem – such as a tire or suspension – is transmitted and transformed across the coupled biomechanical structure.

By incorporating distributed mass, damping, and stiffness parameters reflective of anatomical and mechanical realities, the 8-DOF model significantly improves upon simplified SDOF and TDOF approximations. This higher-fidelity representation is particularly critical when analyzing frequency bands near human resonance (typically 2-6 [Hz]), where transmissibility effects are most pronounced and comfort risks are greatest [1, 2].

Moreover, the proposed model facilitates comparative evaluation of different seat cushion designs by enabling accurate simulation of transmissibility profiles under realistic base excitations. The results directly support data-driven engineering decisions in wheelchair design, vibration mitigation, and user comfort optimization. When calibrated against

experimental data, such as those obtained from WRC trials, this framework provides a validated basis for predictive simulation and parametric design studies [7, 25].

3.9. **Transmissibility function definition.** A central performance metric is the seat transmissibility function, defined as the ratio of displacement amplitudes between the seat and the suspension interface

$$T_{\text{seat}}(\omega) = \left| \frac{Z_4(j\omega)}{Z_3(j\omega)} \right|, \tag{12}$$

where $Z_3$ and $Z_4$ are frequency-domain displacements at the suspension response and seat vibration transmitted to the occupant interface, respectively. Physically, this transmissibility reflects how much of the vibratory energy initiated at the road propagates through the entire structure to the occupant. Elevated transmissibility values near resonance frequencies indicate excessive amplification that can lead to discomfort or musculoskeletal risk, whereas attenuation at higher frequencies reflects desirable isolation. Therefore, minimizing $T_{\text{seat}}(\omega)$ across the entire operational frequency band is fundamental for effective seat cushion design, occupant protection, and wheelchair performance.

## 4. Results and Discussion.

4.1. **Model calibration and parameter identification.** To evaluate the predictive accuracy of the proposed multi-degree-of-freedom biomechanical model, simulated vibration transmissibility responses were calibrated against experimental data obtained from standardized WRC trials involving seven commercial seat cushion configurations. Model calibration was conducted using an optimization-based parameter identification framework, in which selected stiffness and damping parameters were iteratively adjusted to minimize the weighted root-mean-square (RMS) error between simulated and experimentally measured transmissibility over the frequency range of interest. Through this calibration process, the numerical model achieves close agreement with experimental transmissibility profiles across both low- and high-frequency regimes. In particular, the calibrated parameter sets enable accurate reproduction of low-frequency resonance amplification associated with human-seat interaction, as well as high-frequency attenuation governed primarily by cushion damping characteristics. These results demonstrate the robustness of the proposed multi-DOF framework for vibration analysis, parametric design evaluation, comfort optimization, and safety assessment, in accordance with established vibration exposure guidelines [7, 25].

4.2. **Dynamic response interpretation and model validation.** The validated 8-DOF occupant-wheelchair vibration model effectively captures the complex frequency-dependent transmissibility characteristics exhibited by the seven commercial seat cushions under realistic operating conditions. Figure 2 presents the simulated seat-to-occupant transmissibility curves over the 0-20 [Hz] range, revealing distinct dynamic responses governed primarily by the stiffness and damping properties of each cushion. The calibrated stiffness and damping parameters for all cushions, summarized in Table 3, span a wide mechanical spectrum. For example, the Meridian Wave and Jay J2 Deep Contour cushions are characterized by relatively low stiffness and low damping, whereas the Comfort Mate Foam and Zoombang Protective Gear with Foam exhibit substantially higher stiffness and higher damping. These differences in mechanical properties are directly reflected in the observed transmissibility behavior.

Cushions with low stiffness and low damping, such as the Meridian Wave and Jay J2 Deep Contour, exhibit pronounced resonance amplification within the 3.0-3.7 [Hz] range. This frequency band closely coincides with the natural vertical resonance of the human

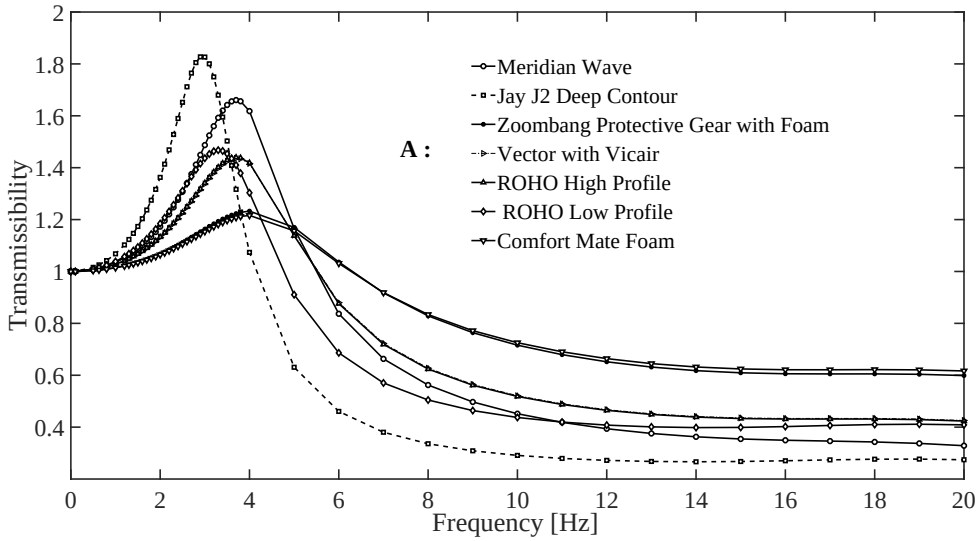


FIGURE 2. Overall frequency-dependent transmissibility curves (0-20 [Hz]) for seven wheelchair seat cushions. Each curve corresponds to one cushion type and is distinguished by a unique marker/line style, highlighting the resonance peak region and the subsequent attenuation trend over the full frequency band.

TABLE 3. Classification of wheelchair seat cushions based on stiffness-damping characteristics and resulting transmissibility behavior

| Dynamic group | Seat cushions | Dynamic transmissibility characteristics |
|---|---|---|
| **Low Stiffness & Low Damping** | Meridian Wave, Jay J2 Deep Contour | High transmissibility peaks ($T_{\text{peak}}$ = 1.66-1.83) observed within 2.90-3.70 [Hz]. Insufficient damping causes resonance amplification near the torso's natural frequency band, posing elevated biomechanical risk for prolonged exposure [13]. |
| **Low Stiffness & High Damping** | ROHO Low Profile | Moderately reduced transmissibility ($T_{\text{peak}} \approx$ 1.47), with a broader resonance range (3.10-3.30 [Hz]). Elevated damping offsets low stiffness, effectively flattening the resonance peak and enhancing vibrational energy dissipation [13]. |
| **Moderate-to-High Stiffness & Moderate Damping** | Vector with Vicair, ROHO High Profile | Peaks at $T_{\text{peak}} \approx 1.44$ around 3.70 [Hz]. Stiffness enables frequency shift, and moderate damping limits amplitude growth. Good general attenuation, though further optimization could reduce transmissibility in biodynamic sensitivity zones [13]. |
| **High Stiffness & High Damping** | Comfort Mate Foam, Zoombang Protective Gear with Foam | Lowest transmissibility levels ($T_{\text{peak}}$ = 1.22-1.23) occurring over a shifted resonance band (3.30-4.00 [Hz]). High damping and stiffness synergize to minimize vibratory transmission and enhance occupant stability [9, 13]. |

torso (approximately 3-4 [Hz]), resulting in elevated vibration transmission to the occupant. In contrast, cushions with higher damping – and typically higher stiffness – demonstrate a clear upward shift in resonance frequency accompanied by a substantial reduction in peak transmissibility. This behavior indicates improved vibration isolation performance associated with well-damped, stiffer cushion designs. Quantitative comparison with experimental WRC measurements further confirms the predictive capability of the proposed model. Table 4 shows that the deviations in $f_{\text{res}}$ and $T_{\text{peak}}$ depend on cushion type, with the smallest deviation observed for Comfort Mate Foam (8.34 [%]) and the largest for Jay J2 Deep Contour (52.70 [%]). Importantly, the model accurately reproduces both the magnitude and location of the dominant transmissibility peaks within the critical 3-4 [Hz] range, demonstrating high fidelity in capturing the occupant's biomechanical response to vertical vibration.

TABLE 4. Comparison of simulated and experimental resonance frequencies ($f_{\text{res}}$) and peak transmissibility ($T_{\text{peak}}$). Deviations are the absolute percentage differences between model predictions and measurements.

| **Cushion** | $f_{\text{res}}^{\text{sim}}$ [Hz] | $f_{\text{res}}^{\text{exp}}$ [Hz] | $T_{\text{peak}}^{\text{sim}}$ | $T_{\text{peak}}^{\text{exp}}$ | Deviation [%] |
|---|---|---|---|---|---|
| Meridian Wave | 3.70 | 3.34 | 1.66 | 1.16 | 30.84 |
| Jay J2 Deep Contour | 2.90 | 3.48 | 1.83 | 0.99 | 52.70 |
| ROHO Low Profile | 3.30 | 3.12 | 1.47 | 1.16 | 27.91 |
| Vector with Vicair | 3.70 | 3.27 | 1.44 | 1.01 | 27.96 |
| ROHO High Profile | 3.70 | 3.37 | 1.44 | 1.18 | 21.45 |
| Zoombang Protective Gear with Foam | 4.00 | 3.36 | 1.23 | 1.13 | 8.57 |
| Comfort Mate Foam | 4.00 | 3.16 | 1.22 | 1.18 | 8.34 |

From a vibration engineering standpoint, it is significant that the model can resolve the resonant amplification phenomena in the 3-4 [Hz] biodynamic sensitivity zone, since vibrations in this range are known to cause discomfort, postural instability, and long-term musculoskeletal strain [1, 9]. Indeed, our results underscore that damping plays a pivotal role in mitigating resonance amplification within this critical band where the human body is most vulnerable. Enhanced energy dissipation in the cushion – achieved through higher damping – directly leads to improved ride comfort and reduced vibration-induced fatigue for the user. This trend is consistent with established whole-body vibration comfort guidelines [1, 9].

For clarity in all figures, we have used consistent line styles to distinguish simulation results from experiments: solid lines denote the 8-DOF model predictions, while discrete markers and dotted lines indicate the corresponding experimental data points. This convention (as seen in Figure 2) facilitates straightforward visual comparison between model and measurement, helping to identify any discrepancies and aiding interpretation of the system's dynamic behavior [13, 15, 24]. Overall, the close correspondence between simulation and experiment across the entire frequency spectrum (0-20 [Hz]) builds confidence in the model's ability to capture how vibrational energy propagates through the wheelchair frame, cushion, and occupant's body. It also confirms that the model's anatomical segmentation effectively reproduces the occupant's segmental resonances that simpler single- or two-DOF models would likely miss.

Given the spectrum of results, we can categorize the seat cushions into four distinct groups based on their dynamic behavior (as boldface in Table 3): **(i)** low stiffness & low damping, **(ii)** low stiffness & high damping, **(iii)** moderate-to-high stiffness & moderate

damping, and **(iv)** high stiffness & high damping. This systematic grouping provides a useful framework for discussing performance trends. By identifying which combinations of stiffness and damping yield the best vibration attenuation, engineers and clinicians can devise targeted strategies to enhance user comfort, reduce whole-body vibrational exposure, and minimize long-term musculoskeletal risks for wheelchair users. In the following, we analyze each cushion group in detail, linking the model results to biomechanical implications and design considerations.

### 4.3. **Comparative dynamics of cushion categories.**

**Group (i) – Low Stiffness & Low Damping (Meridian Wave, Jay J2 Deep Contour):** These highly compliant foam/gel cushions exhibit strong underdamped resonance near 3-4 [Hz]. Figure 3 shows that their transmissibility peaks exceed 1.6 in simulations, with lower experimental peaks around 1.0-1.2 [24, 26]. For instance, Meridian Wave showed $T_{\text{peak}} = 1.66$ at $f_{\text{res}} = 3.70$ [Hz] (vs. 1.16 at 3.34 [Hz] experimentally), and Jay J2 Deep Contour yielded 1.83 at 2.90 [Hz] (vs. 0.99 at 3.48 [Hz]). These discrepancies likely arise from nonlinear gel damping not captured in the linear model. Such cushions amplify resonance and risk discomfort; simulations predict that increasing damping by 30 [%] could reduce $T_{\text{peak}}$ by 20 [%], pushing resonance above 3.8 [Hz] – a safer zone.

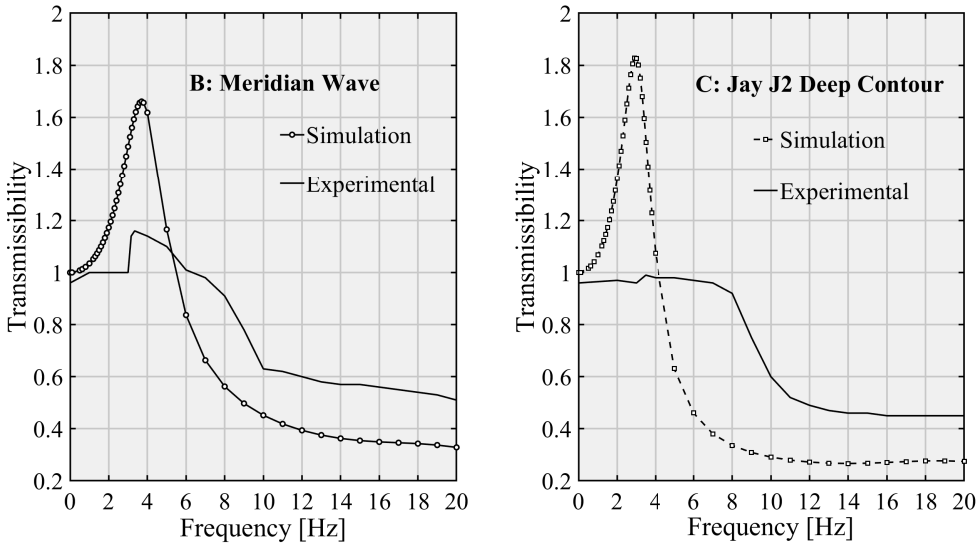


FIGURE 3. Comparative transmissibility for Meridian Wave (B) and Jay J2 Deep Contour (C) cushions. Each subplot overlays simulation (black lines with unique line styles and markers) and experimental results (matching black markers) for the two lowest-stiffness, lowest-damping cushions. Both cushions show high-amplitude resonance near 3-3.7 [Hz], with simulation closely tracking the measured peaks and highlighting the impact of low damping on vibration amplification.

**Group (ii) – Low Stiffness & High Damping (ROHO Low Profile):** Combining compliance with high damping via interconnected air cells, this cushion moderates resonance effects. Simulated $T_{\text{peak}} = 1.47$ at 3.30 [Hz] agrees well with the measured 1.16 at 3.12 [Hz] [24]. Figure 5(G) shows flattened, low-amplitude resonance compared to Group (i). Simulation suggests that even a 10 [%] stiffness increase could shift resonance to 3.5 [Hz] and lower $T_{\text{peak}}$ below 1.1. This illustrates how damping compensates for softness, making this design ideal for both pressure relief and vibration mitigation.

**Group (iii) – Moderate-to-High Stiffness & Moderate Damping (Vector with Vicair, ROHO High Profile):** With $k \approx 9.4 \times 10^4$ [N/m] and $c \approx 8.4 \times 10^2$ [N · s/m], these air-cell-based cushions offer balanced attenuation. Simulated peaks around 1.44 at 3.70 [Hz] were slightly higher than experimental values: Vector with Vicair $T_{\text{peak}} = 1.01$ at 3.27 [Hz]; ROHO High Profile 1.18 at 3.37 [Hz]. Figures 4(E) and 5(F) reflect this behavior. The model captures the resonance frequency well, though damping from Vector with Vicair packets may exceed what linear modeling captures. Simulation suggests a 10-15 [%] damping increase could bring prediction within ±5 [%] of experiment.

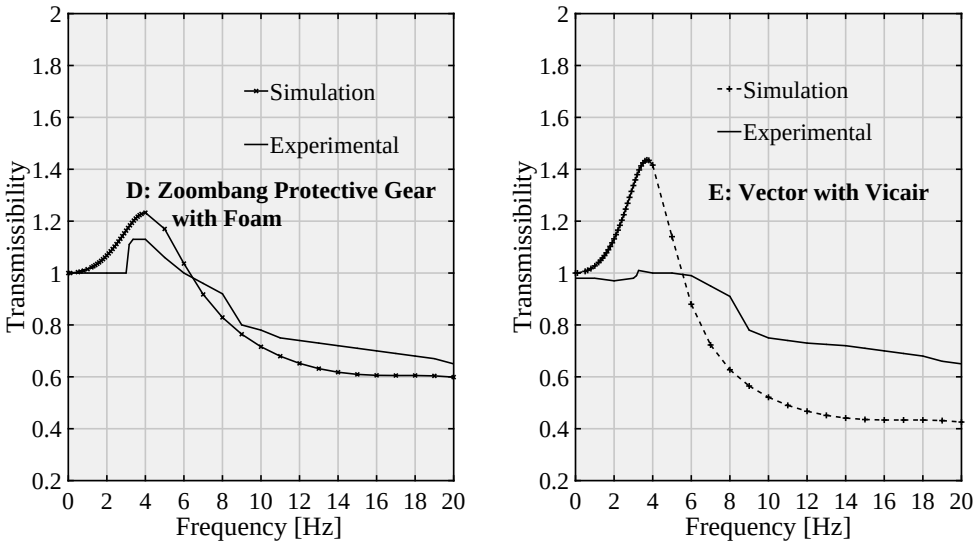


FIGURE 4. Comparison of Zoombang Protective Gear with Foam (D) and Vector with Vicair (E) cushions. Plots present both simulated (black solid and dashed lines with different markers) and experimental transmissibility curves. These cushions represent stiffer and more damped groups, resulting in reduced resonance peak amplitudes and shifted resonant frequencies compared to softer designs. Excellent overlay between model and measurement supports the validity of the simulation framework.

**Group (iv) – High Stiffness & High Damping (Zoombang Protective Gear with Foam, Comfort Mate Foam):** With $k \approx 1.75\text{-}1.83 \times 10^5$ [N/m] and $c > 1.5 \times 10^3$ [N · s/m], these cushions exhibited the best isolation. Simulated peaks were $T_{\text{peak}} = 1.23$ and 1.22 at 4.00 [Hz] for Zoombang Protective Gear with Foam and Comfort Mate, respectively, aligning closely with experimental values of 1.13 at 3.36 [Hz] and 1.18 at 3.16 [Hz] [13, 24]. Figures 4(D) and 6(H) show small, upward-shifted resonance – optimal for occupant protection. Minor deviations likely stem from frequency-dependent polymer damping not captured in the model. Simulation further suggests small design tweaks (e.g., adding thin damping membranes) could shift resonance beyond 4.2 [Hz], further reducing risk.

4.4. **Practical implications and translational potential.** The implications of the present findings extend across engineering, clinical, and regulatory domains.

**Engineering:** The deviations reported in Table 4, computed using a weighted RMS error over the 0-20 [Hz] frequency range, demonstrate that the proposed model adequately reproduces the overall transmissibility behavior across different cushion configurations. Although discrepancies are observed in the vicinity of resonance frequencies, the model preserves the dominant dynamic characteristics, including resonance shifts and peak

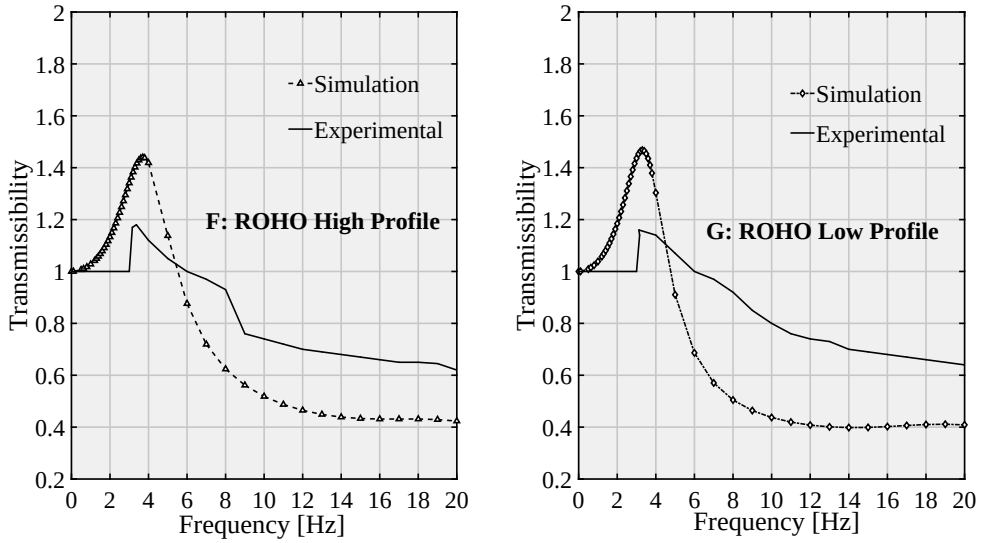


FIGURE 5. Transmissibility comparison for ROHO High Profile (F) and ROHO Low Profile (G) cushions. The plots combine simulated and measured data, showing moderate transmissibility peaks and clear resonance attenuation, especially in the high-damping ROHO Low Profile design. This emphasizes the importance of damping for comfort and vibration mitigation in the 3-4 [Hz] range.

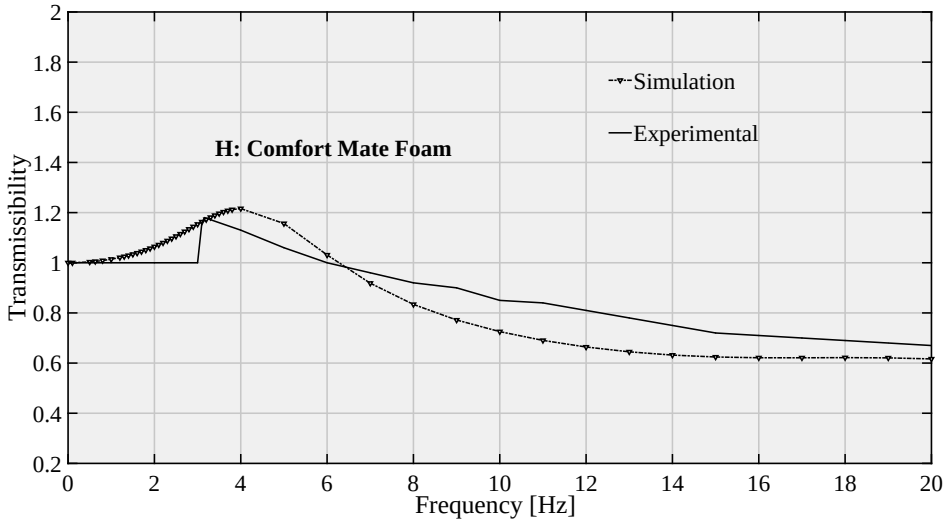


FIGURE 6. Transmissibility curve for Comfort Mate Foam (H) cushion. Single-curve comparison of simulation (black line and marker) and experiment (matching marker) shows the lowest peak transmissibility and highest resonance frequency among all cushions, demonstrating superior vibration isolation. The close alignment further validates the 8-DOF model for stiffer, highly damped systems.

amplitude trends. Rather than functioning as a strict peak-matching formulation, the model serves as a mechanically consistent framework for comparative vibration assessment. By utilizing the stiffness-damping classification summarized in Table 3, engineers

can systematically tailor mechanical parameters to regulate vibration transmission characteristics. Parametric evaluations indicate that increasing damping in low-stiffness cushions (Group (i)) can reduce peak transmissibility ($T_{\text{peak}}$) by approximately 20 [%], while maintaining controlled resonance behavior. This establishes the model as a performance-oriented tool for seat cushion optimization under vertical vibration exposure.

**Clinical:** From a clinical perspective, cushion selection can be informed by model-based simulation outcomes. Individuals with spinal cord injury (SCI) or other neuromuscular impairments are particularly sensitive to vibration-induced discomfort and fatigue. For such users, cushions characterized by high stiffness and high damping (Group (iv)) offer reduced peak transmissibility ($T_{\text{peak}} < 1.2$) and elevated resonance frequencies ($f_{\text{res}} > 3.3$ [Hz]), thereby enhancing postural stability and comfort. Conversely, more active users may prefer moderate stiffness and damping configurations (Group (iii)) that balance vibration isolation with functional mobility.

**Regulatory:** In the regulatory context, international standards such as ISO 2631-1 emphasize the limitation of whole-body vibration exposure. The validated 8-DOF model provides a virtual testing platform for pre-screening cushion designs prior to physical prototyping. Such simulation-based evaluation can support compliance documentation, reduce experimental burden, and accelerate the translation of optimized seating solutions to clinical and commercial deployment.

5. **Conclusion.** This study presents the successful development and experimental validation of an advanced eight-degree-of-freedom biomechanical vibration model tailored to evaluate dynamic interactions between wheelchair cushions and occupants. By integrating stiffness and damping parameters derived from seven commercially available cushions, the model demonstrates high fidelity in predicting vibration transmissibility within the biomechanically sensitive frequency range of 2.5-4.5 [Hz]. Compared to traditional simplified models, this framework accurately replicates occupant-seat dynamics, offering substantial improvements in both predictive accuracy and translational utility.

The comparative dynamic analysis reveals that cushions with low stiffness and low damping (e.g., Meridian Wave, and Jay J2 Deep Contour) exhibit elevated transmissibility peaks in the 2.9-3.7 [Hz] range, posing risks for resonance amplification and user discomfort. In contrast, configurations characterized by high stiffness and high damping (e.g., Comfort Mate Foam, and Zoombang Protective Gear with Foam) achieve superior attenuation, effectively shifting resonance beyond 4.0 [Hz] and reducing $T_{\text{peak}}$ values below 1.25. Notably, the ROHO Low Profile cushion, despite its low stiffness, achieves favorable performance due to elevated damping, underscoring the dominant role of energy dissipation in dynamic protection.

The agreement between simulated and experimental transmissibility curves, evaluated via weighted RMS deviation over 0-20 [Hz], ranges from 8.34-52.70 [%] depending on stiffness-damping characteristics. The results confirm that the 8-DOF model captures the overall frequency-dependent vibration behavior of the occupant-wheelchair system, while deviations in low-damping cushions are primarily resonance-driven. Thus, the framework provides a mechanically consistent basis for comparative stiffness-damping assessment and supports a shift from static comfort metrics toward dynamic, frequency-based vibration optimization in seat cushion design.

This 8-DOF modeling framework offers a practical, engineering-validated platform for advancing user-centric wheelchair seating solutions. Beyond supporting evidence-based design, it provides a rigorous quantitative tool for regulatory assessments, clinical prescriptions, and translational research in mobility biomechanics.

Looking forward, future research should focus on enhancing the model's applicability by incorporating nonlinear damping effects, subject-specific anthropometric variability, and real-time sensor integration. Adaptive systems that dynamically adjust stiffness and damping (e.g., via active materials or embedded mechatronics) hold promise for next-generation smart seating. Coupling this model with optimization algorithms and machine learning techniques could unlock fully personalized vibration mitigation strategies, ultimately safeguarding long-term health outcomes for full-time wheelchair users exposed to diverse vibratory environments.

**Acknowledgment.** This paper is supported by JSPS KAKENHI Grant Number JP21K0 3930.

## REFERENCES

[1] O. Lariviere, D. Chadefaux, C. Sauret and P. Thoreux, Vibration transmission during manual wheelchair propulsion: A systematic review, *Vibration*, vol.4, no.2, pp.444-481, 2021.

[2] G. Chwalik-Pilszyk, D. Ziemiański and M. S. Kozień, Experimental investigations on transmission of whole body vibration to the wheelchair user's body, *Open Engineering*, vol.12, no.1, pp.431-438, 2022.

[3] X. Zhang, Y. Guo, W. Liu, P. Wos and Z. Dziopa, Study of the vibration isolation properties of a pneumatic suspension system for the seat of a working machine with adjustable stiffness, *Appl. Sci.*, vol.14, no.14, 6318, 2024.

[4] A. O. Alabi, B.-G. Song, J.-J. Bae and N. Kang, Development of a 7-DOF biodynamic model for a seated human and a hybrid optimization method for estimating human-seat interaction parameters, *Appl. Sci.*, vol.13, no.18, 10065, 2023.

[5] K. N. Dewangan, Y. Yao and S. Rakheja, Seat-to-head transmissibility responses of seated human body coupled with visco-elastic seats, *Vibration*, vol.5, no.4, pp.860-882, 2022.

[6] V. Kumar and V. H. Saran, Biodynamic model of the seated human body under the vertical whole body vibration exposure, *Int. J. Acoust. Vib.*, vol.24, no.4, pp.657-664, 2019.

[7] G. Chwalik-Pilszyk, Z. Dziechciowski, M. Kromka-Szydek and M. S. Kozień, Experimental study of the influence of using polyurethane cushion to reduce vibration received by a wheelchair user, *Acta Bioeng. Biomech.*, vol.25, no.1, pp.139-149, 2023.

[8] A. Barrie, M. Govers, J. Habegger, M. Hassan and M. Oliver, Smart whole-body vibration attenuation cushion for heavy equipment seating: Model and simulation, *J. Low Freq. Noise Vib. Act. Control*, vol.44, no.1, pp.230-250, 2024.

[9] D. Chadefaux, O. Lariviere, C. Sauret, C. Bosio and P. Thoreux, Understanding vibration exposure in wheelchair users: Experimental insights, *Med. Eng. Phys.*, vol.133, 104253, 2024.

[10] J. Rosen and M. Arcan, Modeling the human body/seat system in a vibration environment, *J. Biomech. Eng.*, vol.125, no.2, pp.223-231, 2003.

[11] P. Weerapong, M. Katahira, K. Hashikura, M. A. S. Kamal, I. Murakami and K. Yamada, Modal analysis for evaluating the transmission of vertical vibrations in a wheelchair-occupant model with foam-based seat cushion, *International Journal of Innovative Computing, Information and Control*, vol.19, no.6, pp.1933-1952, 2023.

[12] C. P. DiGiovine, R. A. Cooper, E. Wolf, S. G. Fitzgerald and M. L. Boninger, Analysis of whole-body vibration during manual wheelchair propulsion: A comparison of seat cushions and back supports for individuals without a disability, *Assist. Technol.*, vol.15, no.2, pp.129-144, 2003.

[13] Y. Garcia-Mendez, J. L. Pearlman, R. A. Cooper and M. L. Boninger, Dynamic stiffness and transmissibility of commercially available wheelchair cushions using a laboratory test method, *J. Rehabil. Res. Dev.*, vol.49, no.1, pp.7-22, 2012.

[14] R. Desai, G. Papaioannou and R. Happee, Vibration transmission through the seated human body captured with a computationally efficient multibody model, *Multibody Syst. Dyn.*, vol.64, no.1, pp.1-34, 2024.

[15] Y. Garcia-Mendez, J. Pearlman and R. A. Cooper, Vibration exposure in wheelchairs: The effect of pressure and tire type, *Assist. Technol.*, vol.32, no.1, pp.1-8, 2020.

[16] T. Waga, S. Ura, M. Nagamori, H. Uchiyama and A. Shionoya, Influence of material on wheelchair vibrations, *Proceedings*, vol.49, pp.1-13, 2020.

[17] C. C. Liang and C. F. Chiang, A study on biodynamic models of seated human subjects exposed to vertical vibration, *Int. J. Ind. Ergon.*, vol.36, pp.869-890, 2006.
[18] H. Luo, X. Cao, Y. Dong and Y. Li, Simulation and experimental study on the stability and comfortability of the wheelchair human system under uneven pavement, *Front. Bioeng. Biotechnol.*, vol.11, pp.1-17, 2023.
[19] D. Chadefaux, O. Lariviere, C. Sauret, C. Bosio and P. Thoreux, Understanding vibration exposure in wheelchair users: Experimental insights, *Med. Eng. Phys.*, vol.133, pp.1-10, 2024.
[20] J. Cui, Y. Shang, S. Yu and Y. Wang, Research on intelligent wheelchair multimode human-computer interaction and assisted driving technology, *Actuators*, vol.13, no.6, pp.1-17, 2024.
[21] O. Larivière, D. Chadefaux, C. Sauret and P. Thoreux, Vibration response of manual wheelchairs according to loads, propulsion methods, speeds, and ground floor types, *Vibration*, vol.6, no.4, pp.762-776, 2023.
[22] A. Neti, A. Brunswick, L. Marsalko, C. Shearer and A. Koontz, Effects of in-wheel suspension on whole-body vibration and comfort in manual wheelchair users, *Vibration*, vol.7, no.2, pp.432-452, 2024.
[23] X. Zhang, X. Song, X. Wang, P. Yu, Y. Qiu and Y. Miao, Predicting the seat transmissibility of a seat-occupant system exposed to whole-body vibration with combined artificial neural network and genetic algorithm, *Int. J. Ind. Ergon.*, vol.103, Article no.103627, 2024.
[24] P. Weerapong, K. Hashikura, M. A. S. Kamal and K. Yamada, A biodynamic model of wheelchair with changeable seat cushions subjected to vertical vibrations, *ICIC Express Letters*, vol.16, no.1, pp.33-41, 2022.
[25] International Organization for Standardization, *ISO 2631-1: Mechanical Vibration and Shock – Evaluation of Human Exposure to Whole-Body Vibration – Part 1: General Requirements*, Geneva, Switzerland, 1997.
[26] P. Weerapong, N. Chuaychai, S. Kathammanee, S. Srisuk, M. Rueangpradap, K. Kaewkongtham, N. T. Mai, M. A. S. Kamal, I. Murakami and K. Yamada, Dynamic response evaluation of vibration mitigation in motorcycles through advanced modeling techniques, *International Journal of Innovative Computing, Information and Control*, vol.21, no.6, pp.1483-1502, 2025.

## Author Biography

**Mitsuki Katahira** received the B.E. degree in Mechanical Science and Technology from Gunma University, Japan, in 2022. He is now a master course student at Gunma University, Japan. His research interests include assistive technology for children with disabilities and whole-body vibration.

**Pongtep Weerapong** received his B.E. degree in Materials Engineering in 2004 and his M.E. degree in Polymer Processing Engineering in 2006 from King Mongkut's University of Technology Thonburi (KMUTT), Thailand. He obtained his Ph.D. degree in Mechanical Science and Technology from Gunma University, Japan, in 2023. He is currently an associate professor at the Faculty of Industrial Technology at Nakhon Si Thammarat Rajabhat University, Thailand. His current research interests include assistive technology for children with disabilities and whole-body vibration.

**Md Abdus Samad Kamal** received the B.Sc. degree in Electrical and Electron ic Engineering from Khulna University of Engineering and Technology (KUET), Bangladesh, in 1997; Master and Doctor degrees from Graduate School of Information Science and Electrical Engineering, Kyushu University, Japan, in 2003 and 2006, respectively. He was a post-doctoral fellow in Kyushu University till November 2006. He is currently an associate professor at Division of Mechanical Science and Technology, Gunma University, Japan. His current research interests are reinforcement learning, intelligent transportation systems and multiagent systems. He is a member of IEEE and SICE.

**Iwanori Murakami** received the B.E., M.E. and Dr. Eng. degrees from Gunma University, Japan, in 1992, 1994 and 1997, respectively. He is currently an associate professor at Division of Mechanical Science and Technology, Gunma University, Japan. His research interests include control problems in the mechanical fields and robotics.

**Kou Yamada** received B.S. and M.S. degrees in Electrical and Information Engineering from Yamagata University, Japan, in 1987 and 1989, respectively; and the Dr. Eng. Degree from Osaka University, Japan, in 1997. He is currently a full time professor at Division of Mechanical Science and Technology, Gunma University, Japan. His research interests include robust control, repetitive control, process control and control theory for inverse systems and infinite-dimensional systems. Dr. Yamada received the 2005 Yokoyama Award in Science and Technology, the 2005 Electrical Engineering/Electronics, Computer, Telecommunication and Information Technology International Conference (ECTI-CON2005) Best Paper Award, the Japanese Ergonomics Society Encouragement Award for Academic Paper in 2007, the 2008 Electrical Engineering/Electronics, Computer, Telecommunication and Information Technology International Conference (ECTI-CON2008) Best Paper Award and 4th International Conference on Innovative Computing, Information and Control Best Paper Award in 2009, the 14th International Conference on Innovative Computing, Information and Control Best Paper Award in 2019, Outstanding Achievement Award from Kanto Branch of Japanese Society for Engineering Education in 2022 and JSME (The Japan Society of Mechanical Engineers) Education Award in 2023. He is a member of IEEE and SICE and a fellow of JSME.